Nair, R. S., Birkemoe, R. C., and Munse, W. H. (1974). "High strength bolts subject to tension and prying." *J. Struct. Div.*, ASCE, 100(2), 351–372.
Packer, J. A., and Morris, L. J. (1977). "A limit state design method for the tension region of bolted beam-to-column connections." *Struct. Engr.*, 55(10), 446–458.
Popov, E. P., and Tsai, K. C. (1987). "Performance of large seismic steel moment connections under cyclic loads." *Proc. 56th Annual Convention*, Structural Engineering Association of California, Oct.
Popov, E. P., Tsai, K. C., and Engelhardt, M. D. (1989). "On seismic steel joints and connections," *Engrg. Struct.*, 11(4), 193–209.
"Recommended testing procedure for assessing the behavior of structural steel elements under cyclic loads." (1986). *Eur. Convention Constr. Steelwork (ECCS), Doc. EECS TWG* 1.3 n. 45/86.
"Specifications for the design, fabrication, and erection of structural steel for buildings," (1989). *Manual of Steel Construction*, 9th Ed., American Inst. of Steel Constr., Chicago, Ill.
Sanpaolesi, L., et al. (1981). "Experimental investigation on strength and ductility of structural connections." *Monographia N. 5, Pubblicazione Italsider, Nuova Italsider*, Genova (in Italian).
Taylor, R. L. (1988). *FEAP—A finite element analysis program*. Dept. of Civ. Engrg., Univ. of California, Berkeley, Calif.
Tsai, K. C. (1988). "Steel beam-column joints in seismic moment resisting frames," dissertation presented to the University of California at Berkeley, Calif., in partial fulfillment of the requirements for the degree of Doctor of Philosophy.

## Appendix III. Conversion to SI Units

| To convert | To | Multiply by |
|---|---|---|
| kip | kN | 4.448 |
| in. | mm | 25.4 |
| kip-ft | kN-m | 1.356 |



# Prestressed Composite Girders under Positive Moment

By Bilal M. Ayyub,[1] Member, ASCE, Young G. Sohn,[2] and Hamid Saadatmanesh[3] Associate Member, ASCE

**Abstract:** According to the 1986 U.S. Federal Highway Administration statistics, there are 575,607 bridges on the highway system. About half of these bridges are structurally deficient and/or functionally obsolete. To strengthen the structurally deficient bridges without replacing the girders, external prestressing techniques can be used. In this paper, the behavior of prestressed, composite steel-concrete beams under positive bending moment is examined, and the benefits of different types of prestressing are compared. These specimens were tested to study various aspects of prestressed composite girders, including tendon type and profile. Two methods of analysis are discussed, i.e., the transformed area method and the strain compatibility method. The test results show that prestressing a composite girder increases the range of elastic behavior, reduces deflections, increases ultimate strength, and adds to the redundancy by providing multiple stress paths. Based on the experimental results, a comparison was made between three tendon types and profiles. It was concluded that strands are more effective than bars for the tendon type, and a straight tendon profile is more effective than a draped profile with regard to stiffness.

## Introduction

The eighth annual report of the Secretary of Transportation to the Congress of the United States on the highway bridge replacement and rehabilitation program (HBRRP) clearly attests to the need for reviving the nation's aging transportation system. According to this report, 40% of the 575,607 inventoried highway bridges in the United States were eligible for HBRRP funding ("Highway" 1986). The condition of the nation's bridges has remained of high priority to the Federal Highway Administration (FHWA) and the state highway agencies. The FHWA recommends that the states, in developing bridge projects, consider the rehabilitation alternative before deciding to replace a structure. An innovative design concept that can be used for retrofitting existing bridges as well as for designing new bridges involves the utilization of prestressing in composite steel-concrete bridges. The main advantages of prestressing follow: (1) To increase the ultimate capacity of the girders; (2) to enlarge the elastic range of behavior; (3) to improve the fatigue strength of the girders with or without existing fatigue cracks; (4) to utilize the material more efficiently, and therefore to reduce the structural steel weight; and (5) to increase the redundancy, and therefore to improve the reliability of the girders. The first advantage results from adding a moment couple consisting of the tension force in the tendon and an equal compressive force in the deck. Second, prestressing induces compressive stresses in the tension flange that delay yielding of the flange. Third, the stresses in

[1]Assoc. Prof., Dept. of Civ. Engrg., Univ. of Maryland, College Park, MD 20742.
[2]Struct. Engr., David Taylor Naval Ship R&D Center, Bethesda, MD 20084-5000.
[3]Asst. Prof., Dept. of Civ. Engrg. and Engrg. Mech., Univ. of Arizona, Tucson, AZ 85721.

Note. Discussion open until April 1, 1991. To extend the closing date one month, a written request must be filed with the ASCE Manager of Journals. The manuscript for this paper was submitted for review and possible publication on October 5, 1989. This paper is part of the ***Journal of Structural Engineering***, Vol. 116, No. 11, November, 1990. ©ASCE, ISSN 0733-9445/90/0011-2931/$1.00 + $.15 per page. Paper No. 25228.

the tension flange can be made to cycle between compression stresses and/or compression low-tension stresses by prestressing. This should improve fatigue life. Fourth, savings in the overall steel weight can be achieved by substituting higher strength strands for lower strength structural steel. Finally, the redundancy of the structure is improved as a result of multiple load paths provided by prestressing tendons. The main objectives of this paper are to present the experimental results and analytical models that predict the stresses in the tendon, concrete deck, and steel beam of prestressed composite girders under positive bending moment.

## Previous Work

In 1949, Dischinger published a series of articles in which he proposed the prestressing of bridges using high-strength cables. (U.S. patent 2-510-958, 1950) and Naillon (U.S. patent 3-010-251, 1961) were separately granted U.S. patents for prestressed composite floor systems and prestressed steel girders, respectively. Szilard (1959) suggested methods for the design and analysis of prestressed composite structures, including the effect of shrinkage and creep of concrete. Hoadley (1963) discussed the behavior of simply supported wide-flange steel beams and composite beams prestressed by using high-strength cables. In 1964, three prestressed composite steel beams subjected to positive bending moment were tested to failure by Strass (1964). Each beam was simply supported and was prestressed with one cable running the full length of the beam below the centerline of the tension flange. Regan (1966) performed an analytical study on the behavior of prestressed composite beams under positive bending moment. The effects of variables such as slab thickness, prestressing force, and load type on the overall behavior of the beams were discussed. In 1968, the subcommittee on prestressed steel of the joint ASCE-AASHTO committee on steel flexural members reviewed previous work in this area and developed analytical models for prestressed steel girders (Ekberg 1968). Klaiber et al. (1982) and Dunker et al. (1986) studied the feasibility of posttensioning composite steel-concrete girders. A bridge model was tested, and the results were compared to a finite element analysis. The agreement between the measured and predicted results was good. Then, the method was used in strengthening two existing bridges in the state of Iowa. Guidelines were also developed for strengthening existing single-span composite bridges. Tochacek and Amrhein (1971) presented the concepts of allowable stresses and factors of safety as applied to prestressed steel structures. In 1986, Saadatmanesh et al. (1989a, b) studied the behavior of prestressed composite steel-concrete beams by testing two beams. One of the beams was tested under positive bending moment and the other beam under negative bending moment. Basu et al. (1987) studied experimentally and analytically the behavior of two-span partially prestressed composite beams. The beams were prestressed in the negative moment region to prevent cracking over the interior support. The concept of prestressed steel has also been studied in Europe, e.g., Bota (1971), Ferjencik and Tochcek (1980), and Ferjencik (1982).

## Experimental Program

Three beams, A, B, and C, were tested to failure under positive bending moment. Five additional beams were also tested to failure under negative



**TABLE 1. Positive Moment Specimens**

| Beam (1) | Section type (2) | Prestressing Tendons: Type (3) | Profile (4) | Position[a] [mm (in.)] (5) | Area [mm² (sq in.)] (6) | Force [kN (kips)] (7) |
|---|---|---|---|---|---|---|
| A | W360 × 45 (W14 × 30) | Bar | Straight | 30.5 (1.2) | 361 (0.56) | 267 (60) |
| B | W360 × 45 (W14 × 30) | Strand | Straight | 30.5 (1.2) | 279 (0.43) | 289 (65) |
| C | W360 × 45 (W14 × 30) | Strand | Draped | 30.5 (1.2) | 279 (0.43) | 267 (60) |

[a]Position of tendon is distance from bottom surface of tension flange at midspan of beam to centroid of tendon.

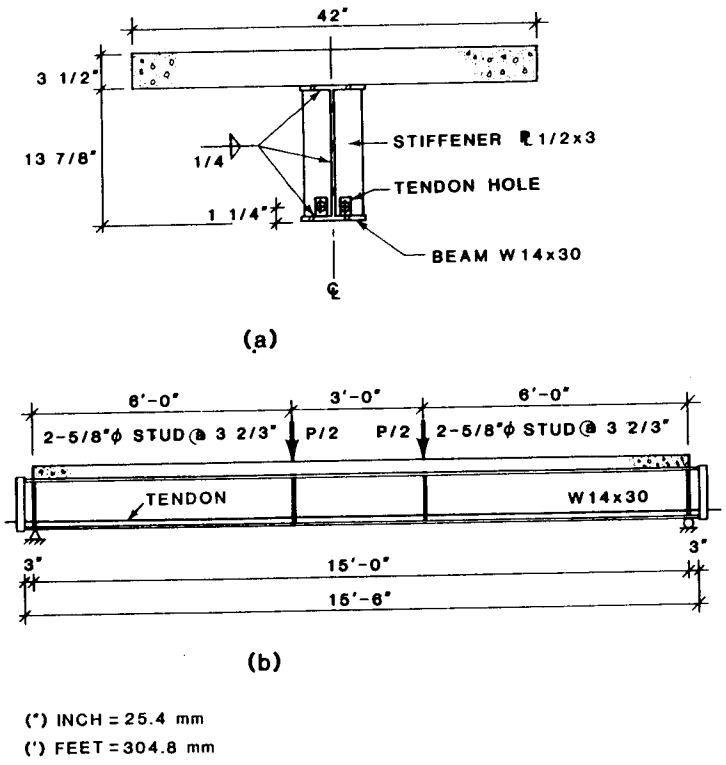


(") INCH = 25.4 mm
(') FEET = 304.8 mm

**FIG. 1. Details of Beams A and B: (*a*) Section; (*b*) Elevation**

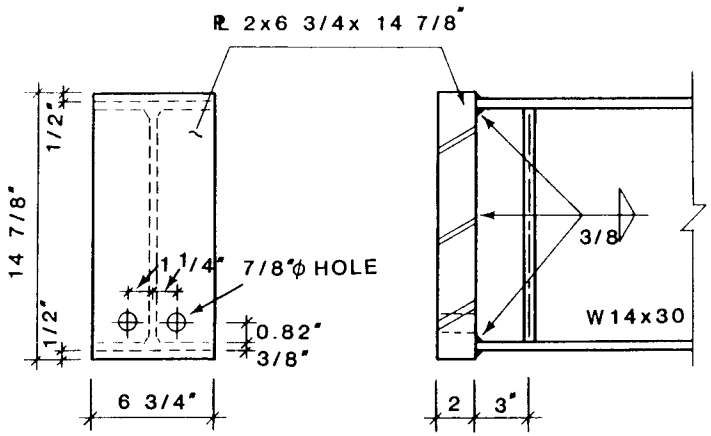


END PLATE DETAIL OF BEAM

(") INCH = 25.4 mm

**FIG. 2. Details of End Plates of Beams A and B**

bending moment. The test results of these five beams are not discussed in this paper. They are described in detail in Ayyub et al. (1988).

After a thorough literature search and analysis, the experimental program for this investigation was designed to study tendon type and profile (Ayyub et al. 1988). Beams A and B were tested to study the differences in the structural behavior between high-strength bars and strands as prestressing tendons. Beams B and C were tested to study the difference in structural behavior between straight and draped tendon profiles. The design parameters of beams A, B, and C are described in Table 1.

## Test Specimens

*Beam A*

As shown in Figs. 1 and 2, beam A consisted of a concrete slab, a steel beam, and two prestressing tendons. The wide flange W360 × 45 (W14 × 30) rolled steel beam had a total length of 4.83 m (15 ft, 10 in.) and was supported on a 4.57-m (15-ft) simple span. The 1.07-m (3.5 ft) wide, 90-mm (3.5-in.) thick, and 4.73-m (15.5-ft) long concrete slab was compositely connected to the steel beam by means of shear stud connectors. The temperature and shrinkage reinforcement consisted of No. 3 [0.375-in., (9.5-mm) diameter] Grade 60 ksi (414 MPa) deformed bars placed in two orthogonal directions. Four pairs of bearing stiffeners were attached to the steel beam at the supports and loading points. The steel beam was prestressed with two 16-mm (5/8-in.) diameter Grade 150 ksi (1,036 MPa) thread bars, each having a nominal cross section of 180 mm$^2$ (0.28 sq in.). The prestressing bars were anchored at the two ends of the beam 30 mm (1.2 in.) above the bottom (tension) flange and were extended on both sides of the



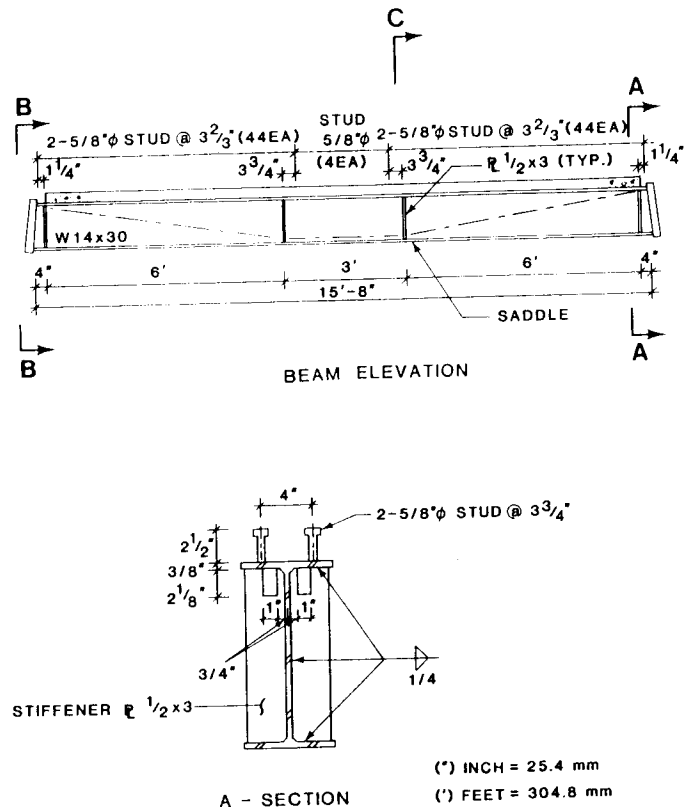


**FIG. 3. Details of Beam C**

web along the full length of the beam. The prestressing was performed before the concrete was cast to prevent the concrete from cracking in tension as a result of a negative moment induced by prestressing.

*Beam B*

This beam is the counterpart of beam A with the same design details except the tendon type. The beam was prestressed with two 15-mm (0.600-in.) diameter, Grade 270 ksi (1,860 MPa) low-relaxation seven-wire strands, running the full beam length 30 mm (1.2 in.) above the bottom (tension) flange.

*Beam C*

This beam was tested to study the effect of draped tendon profiles compared to the straight tendon profile on the structural behavior of the beams. Beam C was similar to beam B and was prestressed with the same strand except with a draped profile, as shown in Fig. 3. The strands were anchored at both ends of the centroidal axis of the composite section, 32 mm (1.25 in.) below the top (compression) flange and were positioned between the

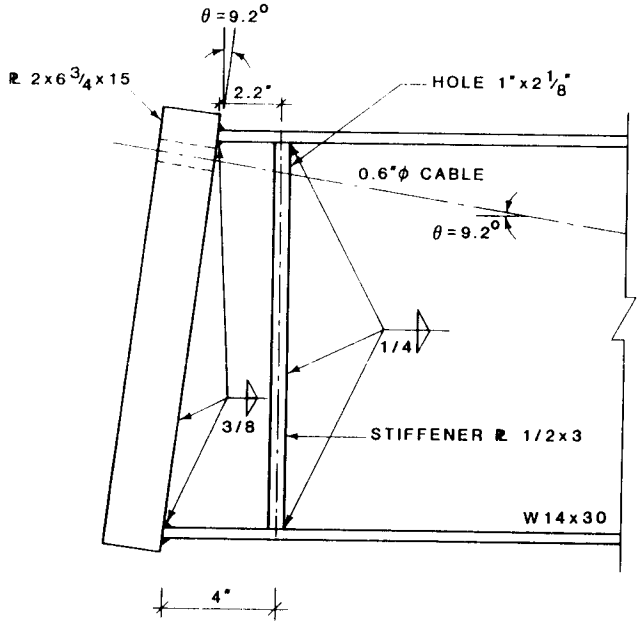


B- END ANCHORAGE OF BEAM

**FIG. 4. Details of End Plates of Beam C**

loading points 30 mm (1.2 in.) above the bottom (tension) flange. Details of the end plates and saddles for beam C are shown in Figs. 3–5.

## Materials

Concrete with the specified design compressive strength of 28 MPa (4 ksi) at 28 days was used for the slabs. Nine concrete cylinders 150 × 305 mm (6 × 12 in.) were cast and tested at the same time as the beams to measure the actual compressive and tensile strengths of concrete. The measured strengths of concrete are summarized in Table 2. Corrosion-resistant, high-strength, low-alloy structural steel, conforming to standard A588 in the *Annual Book of ASTM Standards* (1987) was used for all beams. After testing of beams, three steel coupons were cut from the web of each beam near the support and tested in uniaxial tension to measure the tensile strength properties. These properties are summarized in Table 2. Three samples per beam of high-strength bars and strands were tested in uniaxial tension to measure the yield stress, ultimate strength, and elongation at failure. Table 2 summarizes the measured yield stress and ultimate strength of tendons for each beam. The average elongations at failure of bars and strands were 8.5% and 5.2%, respectively.

## Design of Specimens

To maximize the elastic strength of the prestressed composite beams, a well-proportioned section should be designed, so that concrete and steel reach



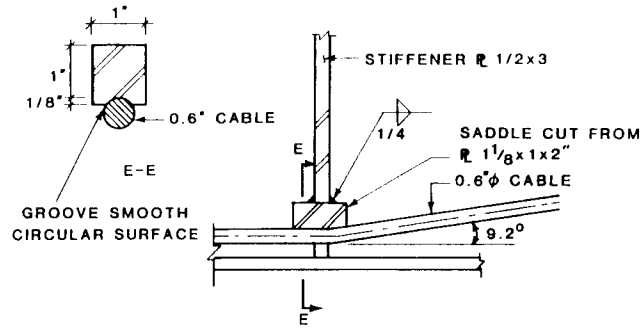


D- CENTER STIFFENER DETAIL

(") INCH = 25.4 mm

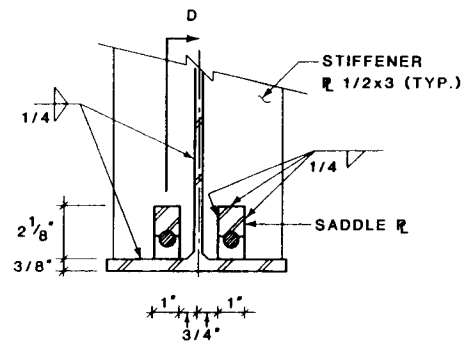


C- SECTION OF BEAM

**FIG. 5. Details of Saddles of Beam C**

**TABLE 2. Mechanical Properties of Materials**

| Element (1) | Mode (2) | Yield Strength: Mean value [MPa (ksi)] (3) | Yield Strength: Standard deviation [MPa (ksi)] (4) | Mean value [MPa (ksi)] (5) | Standard deviation [MPa (ksi)] (6) |
|---|---|---|---|---|---|
| Steel beams | Tension | 411.6 (59.6) | 4.2 (0.6) | 565.4 (82.0) | 2.1 (0.3) |
| Prestressing bars | Tension | 915 (132.4) | 2.8 (0.4) | 1,091 (158.2) | 0.8 (0.1) |
| 15-mm (0.600-in.) strands | Tension | 1,620 (235) | N/A[a] | 2,017 (292) | N/A[a] |
| Concrete | Compression | N/A[a] | N/A[a] | 40.0 (5.8) | 0.63 (0.1) |
| Concrete | Tension | N/A[a] | N/A[a] | 4.0 (0.6) | 0.27 (0.04) |

[a]N/A is either not available or not applicable.

their allowable stresses simultaneously. Based on the working stress and ultimate strength design concepts of AASHTO specifications (*Standard* 1983), various sections of prestressed composite beams were examined analytically. In these analyses, slab size, prestressing force, and the eccentricity of the tendons were considered variable parameters. The results of these analyses were used to determine the cross-sectional dimensions of beams A, B, and C. Shear connectors were also provided in accordance with AASHTO specifications.

### Fabrication of Beams

The steel beams were fabricated in accordance with the AISC fabrication procedures (*Manual* 1980). Shims were utilized to maintain the eccentricity of the tendons in beams A and B, and saddles were welded to the stiffeners for beam C. Bearing plates were used at both ends to distribute the prestressing force and prevent stress concentration.

### Prestressing

The maximum prestressing force was calculated with the interaction equations of AASHTO specifications for beams subjected to axial force and bending moment. The details of the calculations are provided elsewhere (Ayyub et al. 1988).

Steel beam A was prestressed with two thread bars by means of a hydraulic jack. The load was applied alternately in 22.2-kN (5-kip) increments to each bar. The total initial force in each bar after completion of prestressing was 133.4 kN (30 kips). Beams B and C were prestressed by two 15 mm (0.6-in.) diameter strands, using two hydraulic jacks, one at each end. In these beams, the prestressing force was applied simultaneously to both tendons and in one step. The initial force in each tendon of beams B and C after release of the jacks was 173.5 kN (39 kips) and 146 kN (32.8 kips), respectively.

### Instrumentations

All beams were instrumented with electronic measuring devices, and the data were recorded using an automatic data acquisition and reduction system. The strains in the concrete, steel beam, and prestressing bars were measured using electric resistance strain gages. The force in the prestressing strands was measured by means of load cells placed between the end plate and anchorage chucks. The deflection at midspan was measured by two linear variable differential transducers (LVDTs) symmetrically placed on both sides of the web at midspan. The end rotations were measured using clinometers placed at the end plates of the beams. The applied load was measured using an 890-kN (200-kip) capacity load cell.

## Analysis

The transformed area method and the strain compatibility method were used in the analysis. The transformed area method, based on transforming the concrete area into an equivalent steel area, is valid within the elastic limits of the materials. The strain compatibility method, based on the principles of compatibility of deformations and equilibrium of forces, was used to calculate the stresses and deformations at all levels of loading. The ultimate capacity was calculated by assuming complete plastic formation of the section. End rotations and deflection at midspan were obtained by integrating the curvature along the span.



### Assumptions

The following assumptions were made in the analysis: (1) An elastic-fully plastic stress-strain relationship for the steel beam and tendons; (2) a cubic polynomial stress-strain relationship for concrete; (3) a linear strain distribution through the full depth of the composite section; (4) complete composite action, i.e., no slip between the slab and beam; (5) small deformations; (6) constant eccentricity; and (7) unshored construction. The effects of creep, shrinkage, and residual stresses in the steel beams were neglected.

### Increase in Tendon Force

The tendon force in a prestressed composite steel beam increases due to the application of gravity loads. This increase in the tendon force can be calculated by using either the strain energy principle or the compatibility of elongation of the tendon and beam fibers at the level of the tendon at the anchorage points.

To calculate the increase in tendon force by the strain energy method, the total strain energy equation given by Hoadley (1961)

$$U = \frac{1}{2E_sI_s}\int_0^L (M - \Delta Te)^2 dx + \frac{\Delta T^2 L}{2E_sA_s} + \frac{\Delta T^2 L}{2E_tA_t} \quad (1)$$

is differentiated with respect to $\Delta T$. The result is then equated to zero and solved for $\Delta T$, giving

$$\Delta T = \frac{\dfrac{e}{L}\displaystyle\int_0^L M dx}{e^2 + \dfrac{E_sI_s}{E_tA_t} + \dfrac{I_s}{A_s}} \quad (2)$$

where $\Delta T$ = increase in tendon force; $e$ = eccentricity of tendon from centroidal axis of section; $L$ = span of beam; $M$ = applied moment; $E_s$ = modulus of elasticity of steel beam; $E_t$ = modulus of elasticity of tendon; $I_s$ = moment of inertia of steel section; $A_s$ = cross-sectional area of steel beam; and $A_t$ = cross-sectional area of tendons. The integral in Eq. 2 represents the area under the applied moment diagram. The increase in tendon force due to uniformly distributed load $w$ for a straight tendon profile can be derived as a special case of Eq. 2 and is given by

$$\Delta T = \frac{weL^2}{12I_s\left(\dfrac{1}{A_s} + \dfrac{1}{A_t} + \dfrac{e^2}{I_s}\right)} \quad (3)$$

For a draped tendon profile, the compatibility of elongations of the tendon and the beam fibers along the tendon at the anchorage points is used to obtain an expression for $\Delta T$. The elongation of the tendon is given by

$$\Delta_t = \frac{\Delta T}{A_tE_t}[b + 2(a^2 + e^2)^{1/2}] \quad (4)$$

The elongation of the beam fiber at the level of the draped tendon $\Delta_b$ is given by

$$\Delta_b = 2\int_0^a \epsilon_s \frac{x^2}{a^2}\,dx + \epsilon_s b = \epsilon_s\left(\frac{2}{3}a + b\right) \quad (5)$$

The compatibility condition at the anchorage points requires that $\Delta_t = \Delta_b$. Equating Eqs. 4 and 5 and solving for the increase in the tendon force $\Delta T$, the following expression results:

$$\Delta T = \frac{A_t E_t \epsilon_s\left(\frac{2}{3}a + b\right)}{b + 2(a^2 + e^2)^{1/2}} \quad (6)$$

In Eqs. 4–6, $b$, $a$, and $e$ = the distances as shown in Fig. 6; and $\epsilon_s$ = the strain of the beam fiber at the level of the tendon at midspan.

**Transformed Area Method**

The transformed area method is used to determine the stresses and displacements of prestressed composite beams in the elastic region. The cross-sectional properties of the prestressed composite beams are computed after tranforming the concrete into equivalent steel using the modular ratio $n$. The steel beam alone resists the effect of initial prestressing force and dead load. The stress due to dead load and prestressing force at the top of the steel beam is given by

$$f_{2i} = \frac{-T}{A_s} - \frac{\Delta T_D}{A_s} + \frac{M_T C}{I_s} + \frac{\Delta T_D e C}{I_s} - \frac{M_D C}{I_s} \quad (7)$$

and the stress at the bottom of the steel beam is given by

$$f_{3i} = \frac{-T}{A_s} - \frac{\Delta T_D}{A_s} - \frac{M_T C}{I_s} - \frac{\Delta T_D e C}{I_s} + \frac{M_D C}{I_s} \quad (8)$$

where $M_T$ = moment due to prestressing force $T$; $e$ = eccentricity of tendon from centroid of steel beam; $C$ = distance from centroid to extreme fiber of top or bottom flange; $I_s$ = moment of inertia of steel beam; $A_s$ = cross-sectional area of steel beam; $M_D$ = moment due to dead load; and $\Delta T_D$ = increase in tendon force due to applied load. The stress distributions across the depth of the beam due to various components of internal forces are shown in Fig. 7.

The composite section resists the live load plus impact stresses. The transformed area $A_{tr}$ and moment of inertia $I_{tr}$ are used to calculate the stresses in the concrete and the steel beam, as well as the increase in tendon force. The stresses at the top and bottom surfaces of concrete slab $f_{c2}$ and $f_{c1}$ are given by

Top stress:

$$f_{c2} = \frac{1}{n}\left(-\frac{\Delta T_L}{A_{tr}} + \frac{\Delta T_L e_{tr} C_{tc}}{I_{tr}} - \frac{M_L C_{tc}}{I_{tr}}\right) \quad (9c)$$

Bottom stress:

$$f_{c1} = \frac{1}{n}\left(-\frac{\Delta T_L}{A_{tr}} - \frac{\Delta T_L e_{tr} C_{bc}}{I_{tr}} + \frac{M_L C_{bc}}{I_{tr}}\right) \quad (9b)$$



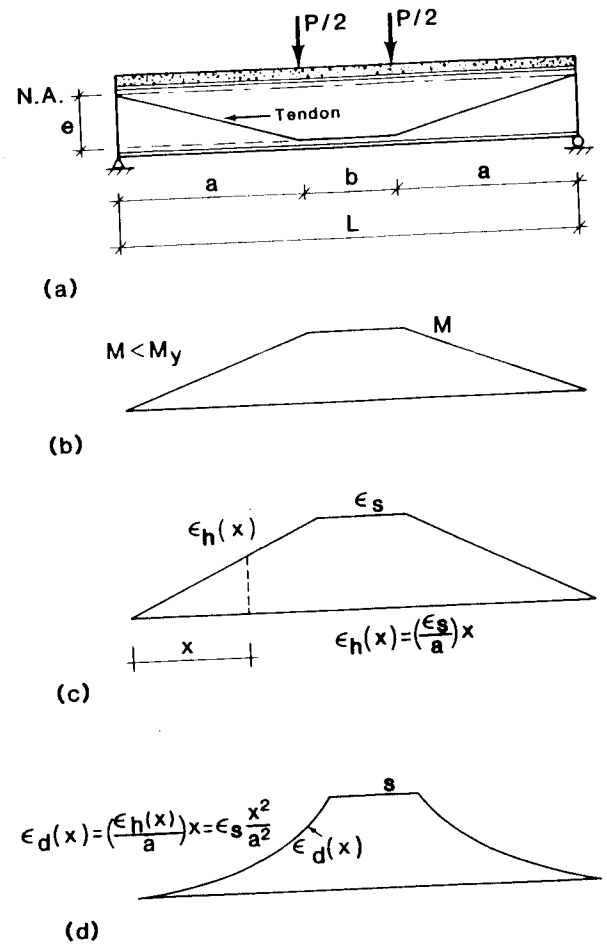


**FIG. 6. Increase in Draped Tendon Force: (*a*) Beam with Applied Load; (*b*) Bending Moment Diagram; (*c*) Strain Diagram of Horizontal Fibers at *e* from Neutral Axis (NA); (*d*) Strain Diagram at Level along Draped Tendon**

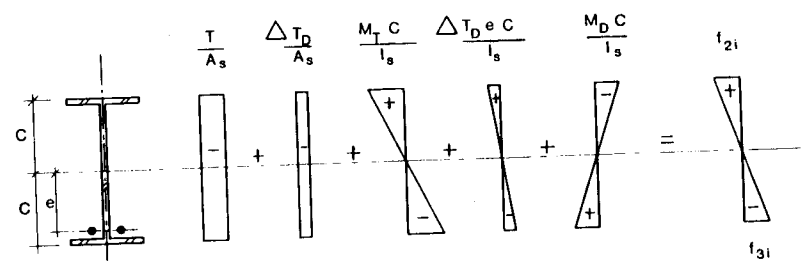


**FIG. 7. Summation of Dead Load Stresses**

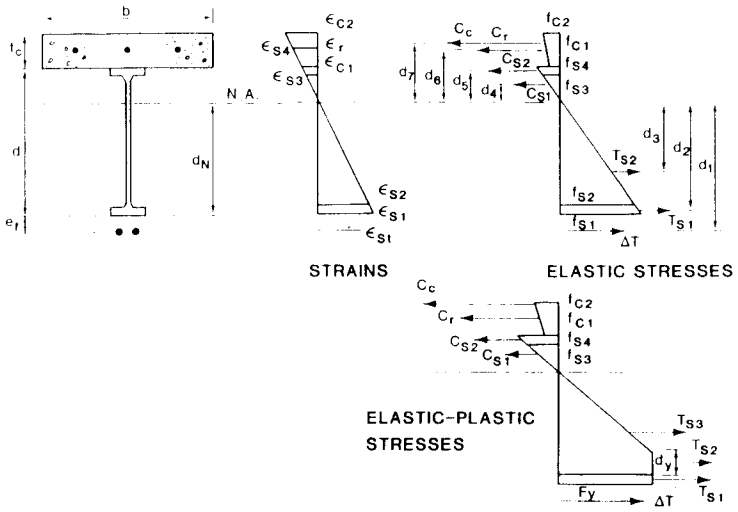


**FIG. 8. Strain and Stress Distribution through Beam Depth (Saadatmanesh et al. 1989)**

where $\Delta T_L$ = increase in prestressing force due to live load $M_L$; $e_{tr}$ = eccentricity of tendon from centroidal axis of composite section; $C_{tc}$ = distance from centroid to top surface of slab; $C_{bc}$ = distance from centroid to bottom surface of slab; $A_{tr}$ = area of transformed composite section; and $I_{tr}$ = moment of inertia of transformed composite section. The total stresses are calculated by superimposing the stresses due to prestressing, dead load, and live loads. The stresses at the top and bottom fibers of the steel beam, $f_2$ and $f_3$, are given by

Top stress:

$$f_2 = f_{2i} + -\frac{\Delta T_L}{A_{tr}} + \frac{\Delta T_L e_{tr} C_{ts}}{I_{tr}} - \frac{M_L C_{ts}}{I_{tr}} \quad (10a)$$

Bottom stress:

$$f_3 = f_{3i} + -\frac{\Delta T_L}{A_{tr}} - \frac{\Delta T_L e_{tr} C_{bs}}{I_{tr}} + \frac{M_L C_{bs}}{I_{tr}} \quad (10b)$$

where $C_{tc}$ = distance from centroid to top surface of steel beam; and $C_{bc}$ = distance from centroid to bottom surface of steel beam. These stresses should be compared to allowable stresses in the AASHTO specifications for design purposes.

### Strain Compatibility Method

A strain compatibility method, based on the principles of equilibrium of forces and compatibility of deformations, is used to determine the state of stresses and deformations in the prestressed composite beams throughout the entire range of loading up to failure.



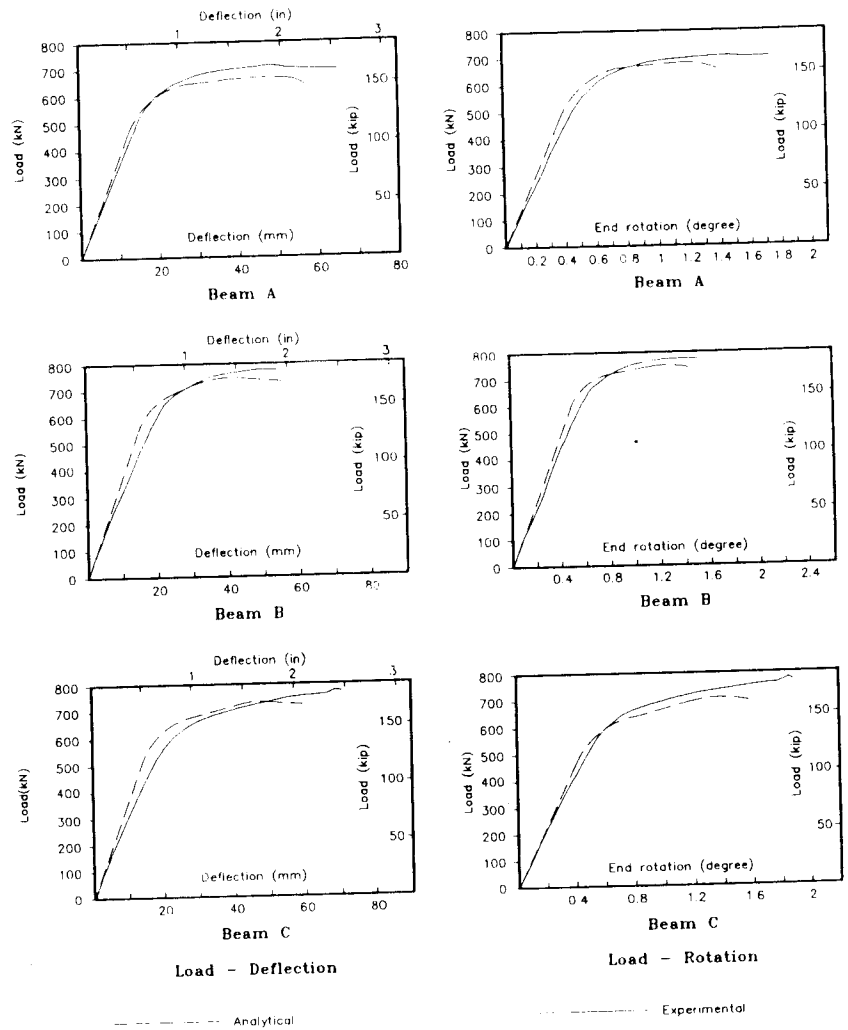


**FIG. 9. Load-Deflection and Load-Rotation Results**

The stress-strain distribution across the depth of the section for the elastic and elastic-plastic state of the stress is shown in Fig. 8 (Saadatmanesh et al. 1989). For ease of calculation, instead of increasing the loads, the strain in the extreme fiber of the tension flange is increased in specified increments. After each increment of strain, the location of the neutral axis is calculated by iterations until the equilibrium of forces across the depth of the cross section is reached. The internal resisting moment is then calculated by summing the moments of all internal forces about the neutral axis. The corresponding applied force is found by equating the internal resisting moment and the moment produced by the applied load. The details of this method are given in Saadatmanesh et al. (1989).

## RESULTS

Beams A, B, and C were tested under positive bending moment. They were tested 31 days, 39 days, and 41 days after casting the concrete, respectively. The experimental results are compared to the corresponding analytical results in the following sections.

### Beam A

The measured load versus deflection curve for beam A is shown with solid lines in Fig. 9. The behavior was initially linear and elastic. The loading and unloading at 356 kN (80 kips) showed a perfect linearity in the load-deflection curve. When the tension (bottom) flange began to yield, the load-deflection curve became progressively nonlinear as yielding progressed into

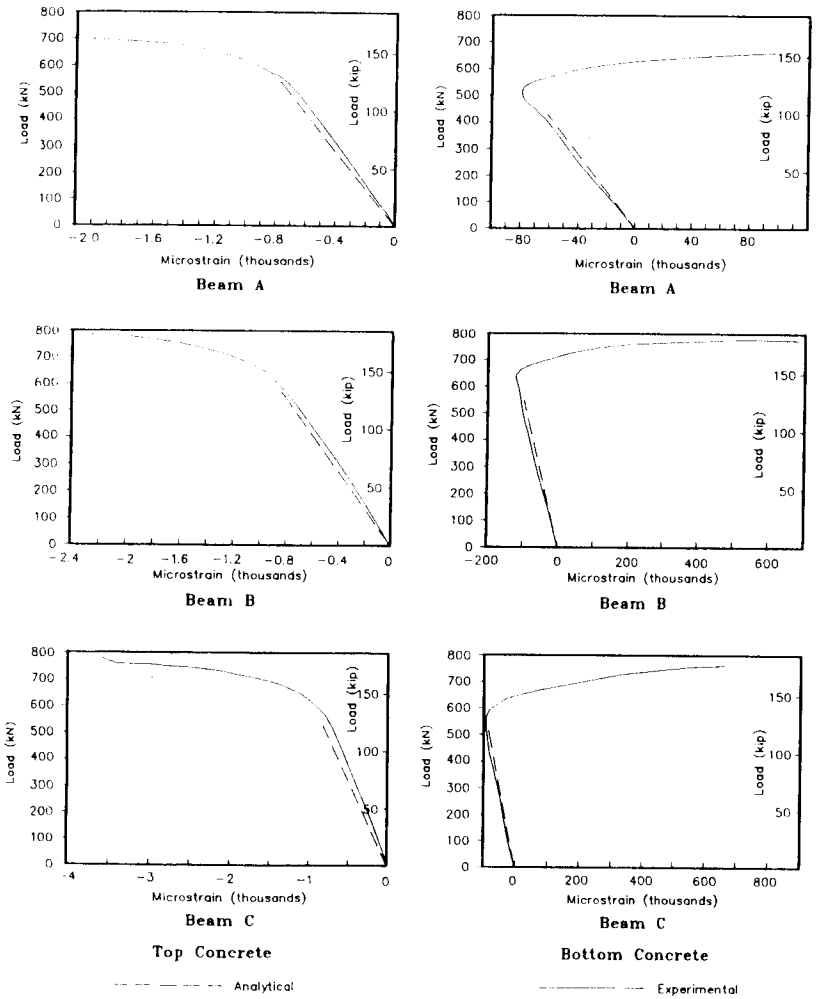


**FIG. 10. Load-Strain Curve for Top and Bottom Concrete**



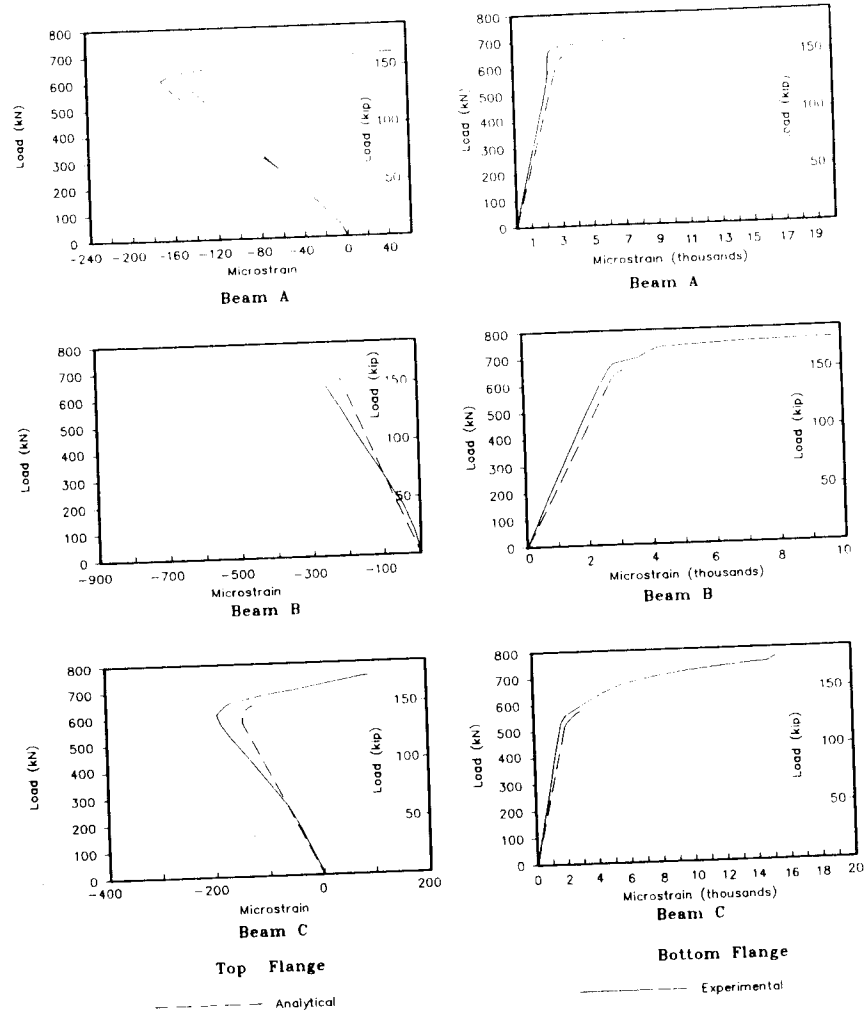


**FIG. 11. Load-Strain Curve for Top and Bottom Flanges of Steel Beams**

the web. At a load of 667 kN (150 kips), the curve showed a plateau because of the reduced beam stiffness due to the yielding of the steel beam and prestressing bars. The predicted load-deflection curve is shown with dashed lines in Fig. 9. The measured and predicted load-deflection curves agree well throughout the entire range of loading. The ultimate strength was calculated by assuming a complete plastic state of stress at midspan. The resulting load is 725 kN (163 kips) and is in reasonable agreement with the measured ultimate load. The measured loads versus end rotations are also shown in Fig. 9. The load-rotation curves are similar to load-deflection curves. The measured and predicted load versus strain in the top and bottom fibers of the concrete at midspan are shown in Fig. 10. The initial behavior was linear and elastic. After the tension flange yielded at a load of about 600 kN (135.4

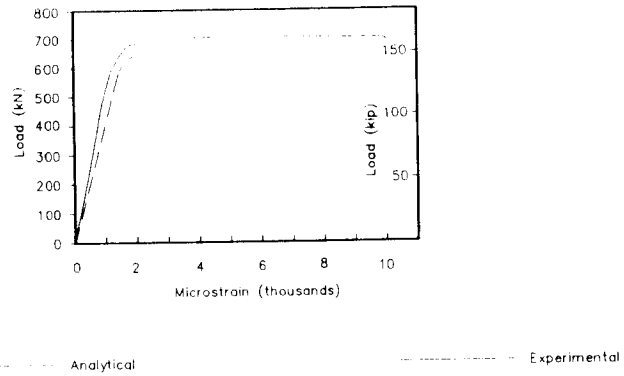


**FIG. 12. Load-Strain Curve for Prestressing Bars of Beam A**

kips), the beam stiffness reduced with nonlinear behavior until concrete crushed locally at a strain of 0.0021. The premature crushing of concrete occurred due to high localized stresses near the loading points. In the elastic region, the centroidal axis of the composite section was located in the steel beam. This resulted in compression stresses in the bottom surface of concrete. After the steel beam yielded, the neutral axis shifted upward, resulting in tension stresses in the bottom surface of the concrete, as shown in Fig. 10. The predicted concrete strains for the top concrete surface, shown with dashed lines in Fig. 10, agreed reasonably well with the measured values. The small deviation between the measured and predicted values can be attributed to incomplete composition action and yielding of shear studs.

Similarly, the measured load versus strain in the extreme fibers of the top (compression) and bottom (tension) flange of the steel beam were plotted and compared with the analytical results. These curves are shown in Fig. 11. The measured load versus strain in the bars is shown with solid lines in Fig. 12. The strain in the bar increased linearly with an increase in the applied load in the elastic range. After the bars yielded at a load of 500 kN (112.4 kips), the slope of the curve slightly reduced. After the tension flange yielded at about 600 kN (135 kips), the stiffness further reduced, and as yielding progressed into the web, the curve flattened more until the ultimate load was reached at crushing of the concrete.

**Beam B**

The load-deflection and load-rotation curves for beam B are shown in Fig. 9. The behavior of beam B was very similar to that of beam A. It was initially linear and elastic. After the tension flange yielded at a load of 623 kN (140 kips), the stiffness reduced and the behavior of the beam became nonlinear until failure was reached by concrete crushing. In this case, the measured load-deflection curve shows less stiffness than the analytical one. This was due to slip between the concrete slab and steel beam and the deformation of shear studs, and also the additional anchorage set of the prestressing strands during the load application. The measured ultimate load for this beam is slightly larger than the calculated one. The difference can be attributed to the strain hardening of steel, which was not considered in the



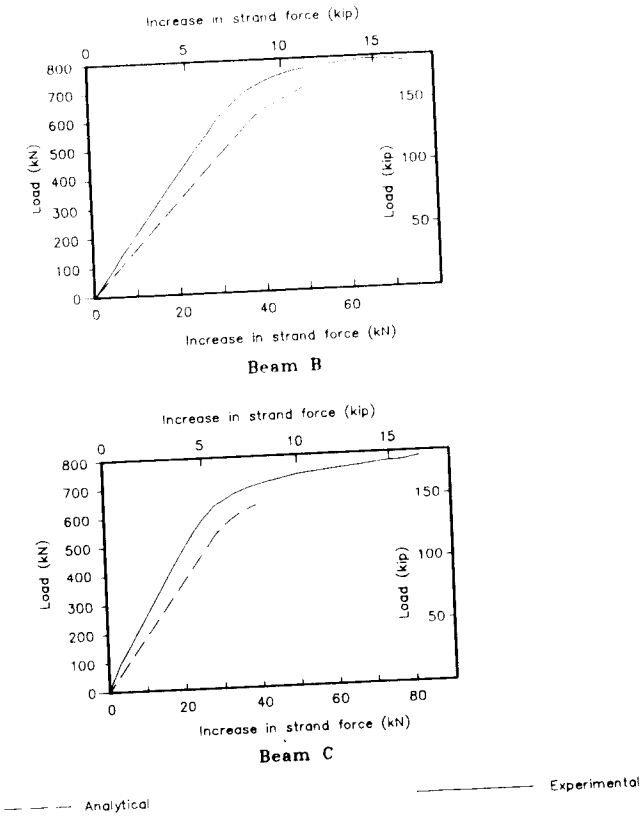


**FIG. 13. Load Increase in Strand Force of Beams B and C**

analysis. The midspan deflection at failure was 56 mm (2.2 in.). This deflection was smaller than that of beam A, 66 mm (2.6 in.), while the ultimate load was slightly larger, indicating that the ductility was less than that of beam A. Fig. 10 shows the load versus strain in the top and bottom fibers of the concrete slab. The load-versus-strain curves in the top (compression) and bottom (tension) flanges of the steel beam are shown in Fig. 11. The tension flange showed large plastic deformation after yielding. Because the compression flange was very close to the neutral axis, it remained elastic throughout the entire range of loading. Fig. 13 shows with solid lines the load versus increase in the strand force. The force in the cable increased linearly with applied load until the tension flange yielded. Thereafter, the behavior became nonlinear until failure by concrete crushing. The predicted curve is shown in Fig. 13 with dashed lines. The difference between the two curves is due to the same reasons discussed for beam A.

**Beam C**

The main feature of beam C is the layout of the prestressing tendons. The measured and predicted load-deflection and load-rotation curves for beam C are shown in Fig. 9. The general behavior of this beam was similar to that

of beam B. However, the tension flange yielded at a smaller load, 534 kN (120 kips), than beam B, 623 kN (140 kips). The ultimate load of this beam was very close to that of beam B. The midspan deflection at failure was 74 mm (2.9 in.), which is more than that of beams A and B, possibly indicating more ductility. Similar to beam B, the measured load-deflection curve for beam C showed less stiffness than the analytical curve, due to incomplete composite action and deformation of shear studs.

The load-versus-strain curves for the top and bottom concrete fibers are shown in Fig. 10. The concrete failed at a strain of 0.0038, which was higher than that of beams A and B. The load versus strain in the bottom fibers started in compression and changed into tension as the neutral axis shifted upward and into the slab. The load-versus-strain curves for the top (compression) and bottom (tension) flanges of the steel beam are shown in Fig. 11. The load versus increase in tendon force is shown in Fig. 13. The tendon forces in beams B and C at failure were almost the same.

### Comparison between Bars and Strands for Prestressing

In this study, high-strength thread bars for beam A and strands for beam B were used as straight steel tendons for prestressing the beams. The prestressing bars are manufactured with a ribbed surface having a minimum tensile strength between 1,000 MPa (145 ksi) and 1,100 MPa (160 ksi). The prestressing strands are produced from seven-wire, high-strength steel. The minimal tensile strength of the strands ranges from 1,725 MPa (250 ksi) to 1,860 MPa (270 ksi). The wedge-type anchorage chuck has a higher set than the nut type bar anchorage, leading to a larger prestress loss.

Based on the general load-deflection behavior of beams A and B, the yield loads of the two beams are almost the same; however, the ultimate load of beam B is much higher than that of beam A. The cross-sectional area of each bar in beam A was 180 $mm^2$ (0.28 sq in.), and the area of each strand in beam B was 139 $mm^2$ (0.216 sq in.). Although the area of the strand was smaller, due to higher strand strength, higher ultimate load was achieved for beam B. Therefore, the use of strands can result in savings in the overall steel weight and can be preferable to using bars as prestressing tendons.

### Comparison between Straight and Draped Tendons

Beam B with the straight tendon profile was compared with beam C with draped tendon profile. The moment produced by the variable eccentric prestressing force nearly counteracts the moment produced by the applied load, and a higher shear resistance is obtained due to the vertical component of the prestressing tendon force in the case of the draped profile. In addition, the draped tendon profile allows more rotation in the beam and, therefore, increases ductility. However, a straight tendon profile results in higher yield load. This enlarges the elastic range of behavior and improves serviceability. Moreover, straight tendons can be more desirable due to their lower construction cost. Thus, the use of the straight tendon profile is more advantageous than that of the draped tendon profile.

## Summary and Conclusions

Three specimens of prestressed composite girders were tested to failure under positive bending moment. An experimental program was developed



to study various aspects of these specimens, including tendon type and profile. Deflections, strains, and increases in tendon force and applied load were measured and compared to predicted values throughout the entire range of loading up to failure.

Two analysis methods were discussed, i.e., the transformed area method and a numerical method based on strain compatibility. The analytical values correlated well with the experimental results.

Based on the experimental results and the analysis of the prestressed composite beams, the following conclusions are drawn.

1. The analytical model based on the compatibility of strains and equilibrium of forces predicts well the stresses and deflections.
2. Prestressing a conventional composite girder can significantly increase the load at which first yielding occurs and the ultimate capacity of the beams.
3. The assumption of zero slip condition may not be justified, because some slip occurred in the tests resulting in larger deflections than predicted.
4. Higher tendon eccentricity results in higher ultimate strength for the beams. Thus, tendons should be located below the bottom (tension) flange, if possible.
5. Larger tendon area for the same prestressing force reduces the deflections and increases the ultimate load of the girder.
6. The use of strands as prestressing tendons is preferable to bars due to their higher strength-to-weight-ratio.
7. Draped tendons increase ductility compared with straight tendons. However, straight tendons can be more desirable due to their lower construction cost.

## Acknowledgment

The writers would like to acknowledge the financial support of the National Science Foundation (Grant Numbers ECE-8413204 and ECE-8513648). Any findings, opinions, conclusions, and recommendations expressed in this publication are those of the writers and do not necessarily reflect the views of the National Science Foundation. The help of Pedro Albrecht in the first stage of the project, as well as the help of Jaykant Parekh in preparing this manuscript, is also acknowledged.

## Appendix I. References

*Annual book of ASTM Standards*. (1987). Am. Soc. for Testing and Materials, Philadelphia, Pa.

Ayyub, B. M., Sohn, Y. G., and Saadatmanesh, H. (1988). "Static strength of prestressed composite steel girders." *Final Report, National Science Foundation, Grant No. ECE-84-13204*, Univ. of Maryland, College Park, Md.

Basu, P. K., Sharif, A. M., and Ahmed, H. U. (1987). "Partially prestressed continuous composite beams I and II." *J. Struct. Engrg.*, ASCE, 113(9), 1926–1938.

Bota, V. (1971). "Calcul en plastisticite des poutres mixtes acier preconstraint-beton." *Romania Constr. Metal*, Institute Polytechnique de Timisoara, 2, 21–34 (in Rumanian).

Dischinger, F. (1949). "Stahlbrucken im verbundmit stahlebeton druckplatten bei gleichzeitiger vorspannung durch hochwertige seite." *Der Bavingerniever*, West Germany, 24(11), 321–332 (in German).

Dunker, K. F., Klaiber, F. W., and Sanders, W. W. (1986). "Post-tensioning distribution in composite bridges." *J. Struct. Engrg.*, ASCE, 112(11), 2540–2553.

Ekberg, C. E. (1968). "Development and use of prestressed steel flexural members."

*J. Struct. Engrg.*, ASCE, 94(9), 2033–2060.
Ferjencik, P. (1982). "Czechoslovak contribution in the field of prestressed steel structures." *Int. Civ. Engrg.*, 2(11), 481–491.
Ferjencik, P., and Tochcek, M. (1980). "Skutocne posobenie predpatych oel'ovych plnostennyh nosnikov." *Stavebnicky Cas*, Czechoslovakia, 28(4), 273–287 (in Czech).
"Highway bridge replacement and rehabilitation program." (1986). *Eighth annual report of the Secretary of Transportation to the Congress of the United States*. Bridge Div., Federal Highway Administration, Washington, D.C.
Hoadley, P. G. (1961). "An analytical study of the behavior of prestressed steel beams," thesis presented to the University of Illinois, at Urbana, Ill., in partial fulfillment of the requirements for the degree of Doctor of Philosophy.
Hoadley, P. G. (1963). "Behavior of prestressed composite steel beams." *J. Struct. Div.*, ASCE, 89(3), 21–34.
Klaiber, F. W., Dunker, K. F., and Sanders, W. W. (1982). "Strengthening of single-span steel beam bridges." *J. Struct. Div.*, ASCE, 108(12), 2766–2780.
*Manual of Steel Construction*. (1980). 8th Ed., Am. Inst. of Steel Constr., Chicago, Ill.
Regan, R. S. (1966). "An analytical study of the behavior of prestressed composite beams," thesis presented to Rice University, at Houston, Tex., in partial fulfillment of the requirements for the degree of Master of Science.
Saadatmanesh, H., Albrecht, P., and Ayyub, B. M. (1989a). "Experimental study of prestressed composite beams." *J. Struct. Engrg.*, ASCE, 115(9), 2349–2364.
Saadatmanesh, H., Albrecht, P., and Ayyub, B. M. (1989b). "Analytical study of prestressed composite beams." *J. Struct. Engrg.*, ASCE, 115(9), 2365–2382.
*Standard specifications for highway bridges*. (1983). 13th Ed., Am. Assoc. of State Highway and Transp. Officials, Washington, D.C.
Strass, J. C. (1964). "An experimental and analytical study of prestressed composite beams," thesis presented to Rice University, at Houston, Tex., in partial fulfillment of the requirements for the degree of Master of Science.
Szilard, R. (1959). "Design of prestressed composite steel structures." *J. Struct. Div.*, ASCE, 85(9), 97–123.
Tochacek, M., and Amrheim, F. G. (1971). "Which design concept for prestressed steel." *AISC Engrg. J.*, 8(1), 18–30.

## Appendix II. Notation

*The following symbols are used in this paper:*

$A$ = cross-sectional area;
$a$ = fraction of beam length between loading points;
$b$ = distance from loading point to anchorage;
$C$ = distance from centroid to point within section;
$dx$ = differential;
$E$ = elastic modulus of elasticity;
$e$ = eccentricity from centroid of tendon to steel beam;
$f$ = stress;
$f'$ = compressive strength;
$I$ = moment of inertia;
$L$ = span length of beam;
$M$ = moment;
$n$ = modular ratio;
$T$ = prestressing force;
$U$ = total strain energy;
$w$ = uniform gravity load;
$x$ = distance along span;



$\Delta T$ = increase in tendon force; and
$\epsilon$ = strain.

**Subscripts**

$b$ = bottom fibers;
$bc$ = bottom of concrete slab;
$c$ = concrete slab;
$c1$ = top surface of slab;
$c2$ = bottom surface of slab;
$D$ = dead load;
$L$ = live load;
$s$ = steel beam;
$T$ = tendon force;
$t$ = tendon;
$tc$ = top of concrete slab;
$tr$ = transformed section;
$2i$ = top of steel beam due to prestressing and dead load; and
$3i$ = bottom of steel beam due to prestressing and dead load.